Partanen, Iida; Al-Saedy, Omar; Eskelinen, Toni; Karttunen, Antti J.; Saarinen, Jarkko J.; Mrózek, Ondrej; Steffen, Andreas; Belyaev, Andrey; Chou, Pi-Tai; Koshevoy, Igor O.

Fast and Tunable Phosphorescence from Organic Ionic Crystals

Published in:
Angewandte Chemie - International Edition

DOI:
10.1002/anie.202305108

Published: 04/09/2023

Document Version
Publisher's PDF, also known as Version of record

How to cite: *Angew. Chem. Int. Ed.* **2023**, *62*, e202305108
doi.org/10.1002/anie.202305108

Organic Crystals Hot Paper

Fast and Tunable Phosphorescence from Organic Ionic Crystals

Iida Partanen, Omar Al-Saedy, Toni Eskelinen, Antti J. Karttunen, Jarkko J. Saarinen, Ondrej Mrózek, Andreas Steffen, Andrey Belyaev,* Pi-Tai Chou,* and Igor O. Koshevoy**

Abstract: Crystalline diphosphonium iodides [MeR_2P-spacer-R_2Me]I with phenylene (**1**, **2**), naphthalene (**3**, **4**), biphenyl (**5**) and anthracene (**6**) as aromatic spacers, are photoemissive under ambient conditions. The emission colors (λ_{em} values from 550 to 880 nm) and intensities (Φ_{em} reaching 0.75) are defined by the composition and substitution geometry of the central conjugated chromophore motif, and the anion-π interactions. Time-resolved and variable-temperature luminescence studies suggest phosphorescence for all the titled compounds, which demonstrate observed lifetimes of 0.46–92.23 μs at 297 K. Radiative rate constants k_r as high as 2.8×10^5 s^{-1} deduced for salts **1**–**3** were assigned to strong spin-orbit coupling enhanced by an external heavy atom effect arising from the anion-π charge-transfer character of the triplet excited state. These rates of anomalously fast metal-free phosphorescence are comparable to those of transition metal complexes and organic luminophores that utilize triplet excitons via a thermally activated delayed fluorescence mechanism, making such ionic luminophores a new paradigm for the design of photofunctional and responsive molecular materials.

[*] I. Partanen, O. Al-Saedy, Prof. J. J. Saarinen, Prof. I. O. Koshevoy
Department of Chemistry, University of Eastern Finland
Yliopistokatu 7, 80101 Joensuu (Finland)
E-mail: igor.koshevoy@uef.fi

Dr. T. Eskelinen, Prof. A. J. Karttunen
Department of Chemistry and Materials Science, Aalto University
00076 Aalto (Finland)

Dr. O. Mrózek, Prof. A. Steffen, Dr. A. Belyaev
Department of Chemistry and Chemical Biology, TU Dortmund University
Otto-Hahn-Str. 6, 44227 Dortmund (Germany)
E-mail: andreas.steffen@tu-dortmund.de

Dr. A. Belyaev
Department of Chemistry/Nanoscience Center, University of Jyväskylä
Survontie 9C, 40014 Jyväskylä (Finland)
E-mail: andrei.a.beliaev@jyu.fi

Prof. P.-T. Chou
Department of Chemistry, National Taiwan University
Taipei, Taiwan 10617 (ROC)
E-mail: chop@ntu.edu.tw

Introduction

Harvesting phosphorescence from organic materials under ambient conditions is a fundamentally challenging but appealing research task, and success will have promising potential for advancing many fields in energy and materials sciences related to light generation.[1] An intrinsic feature of the vast majority of organic luminophores is small spin-orbit coupling (SOC), which results in very slow rates of intersystem crossing (ISC) $S_n\rightarrow T_n$ and of radiative relaxation $T_1\rightarrow S_0$ thus preventing efficient triplet emission. Spin-forbidden electronic transitions can be substantially facilitated at the molecular level by employing motifs with non-bonding electron pairs (e.g. carbonyl,[2] cyano,[3] sulfur[4] and phosphorus derivatives,[5] and N-heterocycles[6]) that provide orbital changes for the singlet and triplet states to promote SOC (El-Sayed rule). Using this approach, diverse metal-free molecular materials exhibiting room-temperature phosphorescence have been obtained. These species predominantly exhibit long lifetimes from milliseconds to seconds, which is indicative of relatively low SOC values and moderate quantum yields owing to competing non-radiative decays. On the other hand, bringing heavy atoms in close proximity to the chromophore center can increase k_{ISC}, which is proportional to Z^8/r^6, where Z and r denote the atomic number and the distance to the emissive motif, respectively. In this strategy, heavy elements (Br, I) are covalently tailored to the main organic core.[7] The intensity of phosphorescence can be boosted by embedding the emitter into a rigidifying host to suppress non-radiative relaxation,[8] or the heavy atom effect (HAE) can be combined with the simultaneous manipulation of the angular momentum, for example, by incorporating Se into the chromophore.[9] Alternatively, the HAE can be introduced intermolecularly, for instance by means of stacking,[10] halogen bonding[11] or electrostatic attraction in ionic dyes.[12] The latter methodology offers a way to tune the optical characteristics of materials not only by modulating the chemical structure of the emissive cation, but also by adjusting the external HAE, that is, by varying the nature of the heavy anion and the charge transfer (CT) cation-anion interactions. Recently, a series of readily accessible delayed fluorescent, phosphorescent and long-persistent luminescent arylphosphonium compounds were reported by several groups.[13] In particular, it has been shown that the halide counterion in carbazolyl-containing phosphonium salts allows for adjusting both the radiative rate of the $T_1\rightarrow S_0$ decay ($k_r\approx0.7$ $s^{-1}/\tau=112$ ms for the chloride and k_r

$\approx 4.6\ s^{-1}/\tau = 17$ ms for the iodide, with Φ_{em} up to 0.078) and the ratio of fluorescence vs phosphorescence, attaining white light emission.[14] The combination of an external HAE and a small S_1-T_n energy gap in accelerating the emission, which utilizes the triplet state and improves its quantum efficiency, has been proposed for simple tri- and tetraphenyl phosphonium halides. These exhibit gradual shortening of the excited state lifetime from hundreds of milliseconds for $[RPh_3P]Cl$ to a few microseconds for $[RPh_3P]I$ (R = Me, Ph).[15] In contrast to the majority of metal-free phosphors with long and ultralong emissions, these salts are among the few rare organic phosphors that have very fast radiative decays ($k_r \approx 10^4$–$10^5\ s^{-1}$),[16] which are comparable to those of transition metal luminophores.

Inspired by the exceptionally fast delayed photoluminescence behavior of aryl phosphonium iodides at room temperature, we aimed to generalize this concept and investigated the efficiency of harvesting the triplet state from ionic crystalline materials. Donor-acceptor phosphonium salts demonstrate prompt fluorescence effectively quenched in the presence of I^- counterion,[17] a long persistent afterglow, as exemplified by [*p*-Me_2N-C_6H_4-PPh_2Pr]Br,[13d] or intra-cation delayed fluorescence, which was shown recently for [*p*-acridinyl-C_6H_4-PPh_3]X.[13e] Thus, we hypothesized that (*i*) easy to prepare and quaternize tertiary bisphosphanes with different conjugated substituents could provide tunability of the excited state dynamics and triplet state energy (i.e., of the emission wavelength) and that (*ii*) we could possibly enhance the external HAE and anion-π charge transfer[12e,18] by increasing the electrostatic attraction (i.e. shortening the cation-anion distance) by employing dicationic chromophore components.

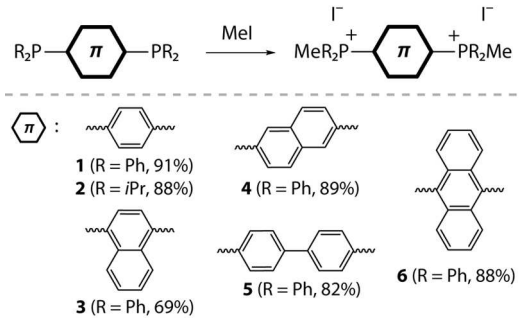

Scheme 1. Synthesis of diphosphonium iodides **1**–**6**.

Results and Discussion

Synthesis and Structural Characterization

The target diphosphonium iodides **1**–**6** (Scheme 1) were conventionally synthesized from previously described tertiary bisphosphanes containing conjugated spacers (phenylene,[19] biphenyl,[19a] naphthalene,[20] and anthracene[21]) by treatment with excess methyl iodide (see details in the Supporting Information). Derivative **1**[OTf] was prepared by reacting 1,4-bis(diphenylphosphino)benzene with methyl triflate. All salts were isolated as uniform crystalline materials after several recrystallization cycles, except for compound **2**, the bulk microcrystalline solid of which was obtained directly from the reaction mixture. The crystalline materials exhibited good thermal stabilities up to ca. 620 K (Figure S1). The composition and purity of the samples were confirmed using NMR spectroscopy and elemental analysis. The ^{31}P NMR spectra display single resonances in the low-field region (20.6–43.5 ppm), which indicate the complete methylation of the phosphane groups and symmetric structures for the resulting dications.

All title salts were studied using X-ray diffraction (Tables S1 and S2 list the crystal data and selected molecular parameters).[22] Crystallographic data confirmed the expected structures of the organophosphorus cations, in which two -PR_2Me groups were appended to the aromatic cores (Figure 1). Compound **1**[23] was isolated in two main forms, the dichloromethane (**1**$^{\mathbf{D}}$) or diethyl ether (**1**$^{\mathbf{E}}$) solvates depending on the solvents used, with the latter typically containing small amounts of solvent-free form **1** (Figures 1 and S2). Both solvates crystallized in the same type of the spacegroup ($P2_1/n$) with similar unit cell parameters. Upon vacuum drying **1**$^{\mathbf{D}}$ and **1**$^{\mathbf{E}}$ gave micro-

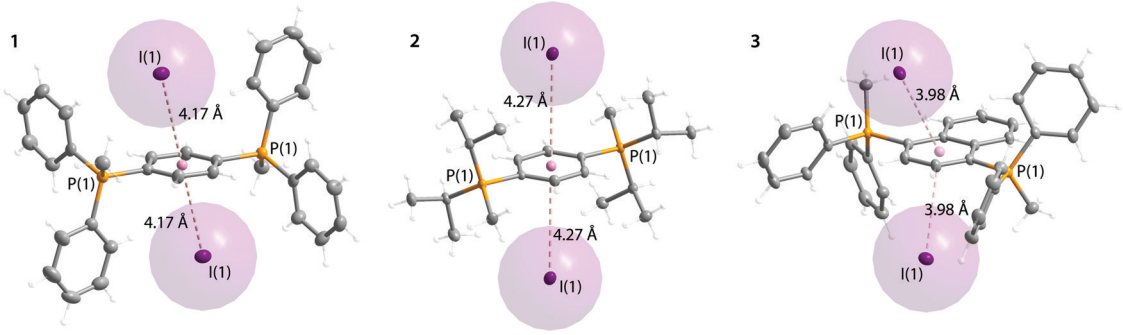

Figure 1. Ion pairs of **1**, **2** and **3** featuring the shortest anion-π contacts with a spacer between P atoms (crystallization methanol molecule in **3** is omitted for clarity; thermal ellipsoids are shown at the 50% probability level; the ellipsoids of iodine atoms are superimposed with space-filling spheres).

crystalline materials with essentially identical optical behaviors, and their powder diffraction patterns conformed to that of the non-solvated modification (Figure S3). Compound **2** was structurally analyzed to be a water solvate $\mathbf{2}^{\mathbf{w}}$ and the non-solvate **2**. According to the PXRD data (Figure S3), form **2** was crystallographically identical to the microcrystalline bulk solid precipitated from the reaction mixture in dichloromethane.

Common features of **1**–**3** include short anion-π contacts.[24] The spacers of the diphosphonium cations are sandwiched between the iodide counterions in a symmetric fashion with I···π(centroid) distances of 3.98–4.27 Å (Figure 1), and the anion-π vectors form angles of ca. 21° (**1**), 16° (**2**) and 26° (**3**) to the ring normals. Such cation-anion organization together with bulky and electron-withdrawing -PR_2Me substituents prevents π-π stacking of the $[P\text{-}\pi\text{-}P]^{2+}$ fragments but presumably facilitates the formation of anion-π charge transfer complexes.[25] The cation-anion arrangement of the triflate salt **1**[OTf], where the phenylene fragment is embedded between the sulfonate groups of the adjacent $CF_3SO_3^-$, resembles that of **1** (Figure S4).

The crystal structures of **4** and **5** do not manifest short anion–π contacts (Figures 2 and S5). Instead, in **4**, the naphthalene and the closest iodides lie almost in the same plane giving rise to C–H···I hydrogen bonds. In **5**, the anions that surround the biphenyl fragment form a trigonal-like geometry (Figure S5) with significant displacement from the aromatic π-system and rather long I···centroid separations (4.91–5.15 Å). This geometry does not favor efficient anion-π interactions, which occur when the distances to the carbon atoms from the anion, located above the π-ring, are shorter than the sum of van der Waals radii +0.8 Å,[24a] i.e. ≤4.48 Å for an I···C pair.

In the case of **6**, the I···π interaction is observed from one side of the curved anthracene motif at the I···centroid distance of 3.70 Å (Figure 2) and I···C(central ring) separations from 3.86 to 4.08 Å.

Photophysical Properties

Solution behavior. The absorption spectra of compounds **1**–**6** measured in methanol/dichloromethane solutions (1:1 v/v mixture, Figure 3, Table S3) display low-energy bands with distinguishable vibrational progressions, which correspond to the π-π* character of electronic transitions. TD-DFT analysis confirmed that vertical $S_0 \rightarrow S_1$ excitations occured within spacers bearing $-^{+}PPh_2Me$ groups, with some participation of P–C orbitals (Figure S6, Table S4). The peak wavelengths were red shifted with an increase in

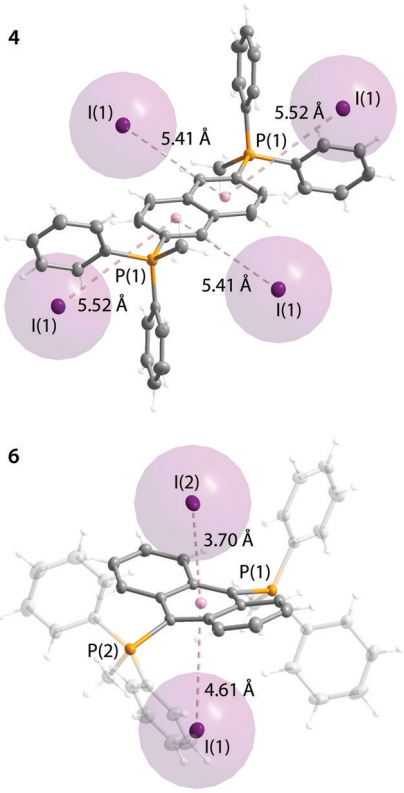

Figure 2. Ion pairs of **4** and **6** featuring shortest anion-π contacts with the spacer between P atoms (crystallization methanol molecules are omitted for clarity; thermal ellipsoids are shown at the 50% probability level; the ellipsoids of iodine atoms are superimposed with space-filling spheres).

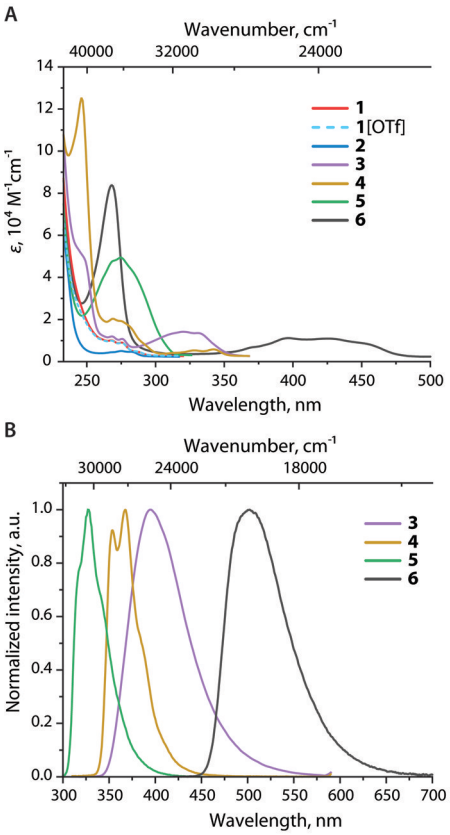

Figure 3. A) UV/Vis absorption spectra of salts **1**–**6** and **1**[OTf]. B) normalized emission spectra of **3**–**6** in methanol/dichloromethane solutions (1:1 v/v mixture, 297 K).

the conjugated system of the aromatic fragments. This reflects the stabilization of the LUMO levels and the corresponding reduction in the optical band gap. The absorption profiles of **1** and its triflate analog **1**[OTf] were nearly indistinguishable and appreciable ion pairing was excluded at low concentrations in polar solvents.

Under UV irradiation ($\lambda_{exc}=275$ nm), diphosphonium salts **1**, **1**[OTf] and **2** with 1,4-substituted phenylene spacer were non-emissive in solution, whereas weak-to-moderate fluorescence in the 317–395 nm region was detected for compounds **3**–**5** (Figure 3, Table S3). The luminescence for anthracene-based salt **6** ($\lambda_{em}=500$ nm, $\Phi_{em}=0.57$, $\tau=6.2$ ns) was substantially stronger than that for **1**–**5** and bathochromically shifted by $\Delta\nu=1413\ cm^{-1}$ compared to its bis(oxophosphorane) congener ($\lambda_{em}=467$ nm, $\Phi_{em}=0.48$ in MeOH).[26] These emissions in solution likely originate from the $^1\pi$-π^* excited states as illustrated by the electron density plots for $S_1\rightarrow S_0$ transitions (Figure S6).

Solid-state behavior. In the crystalline state, the photophysical properties of **1**–**6** are governed not only by the structural features of the cations, but also by non-covalent interactions defined by crystal packing. To ensure uniformity of the samples, materials containing the crystallization solvent were thoroughly evacuated prior to the photophysical studies.

Crystalline samples **1** and **3**–**6** were visibly colored (Figure S7), and the absorption bands of **3** and **6** extended to 550 and 700 nm, respectively. In the absence of π-π stacking involving aromatic spacers of the cations, as confirmed by the XRD data, these low energy absorptions imply the formation of ground state iodide-π charge transfer complexes.[24b,27]

In contrast to the non-emissive behavior of **1** and **2** in a fluid medium at room temperature, the microcrystalline materials **1** and **2** are bright yellow to greenish luminophores showing broad signals at 560 (**1**) and 520 nm (**2**) with remarkably high quantum yields of 0.54 (**1**) and 0.75 (**2**) (Figure 4 and Table 1). The emission lifetimes for both compounds were evaluated using a biexponential fit ($\tau_{av}=2.13$ and 2.71 μs for **1** and **2**) and had corresponding radiative rate constants k_r as high as $2.54\times10^5\ s^{-1}$ (**1**) and $2.77\times10^5\ s^{-1}$ (**2**), respectively. The luminescence of the yellow crystals of salt **3** containing 1,4-substituted naphthalene was bathochromically shifted to 645 nm owing to extension of the central fragment (Figure 4).

The decrease in the quantum yield ($\Phi_{em}=0.07$) was accompanied by a shortening of the average observed lifetime to 0.46 μs. The radiative rate k_r for **3** is $1.64\times10^5\ s^{-1}$, which is still in the order of magnitude found for **1** and **2**. The lower luminescence intensity of **3** is primarily attributed to a more efficient non-radiative relaxation.

Compounds with 2,6-naphthalene (**4**), 4,4′-biphenyl (**5**), and 9,10-anthracene (**6**) spacers form another group of luminophores. The room temperature emission spectra of **4** and **5** revealed a vibrational structure that was barely discernible for **6** but was well resolved for all three species

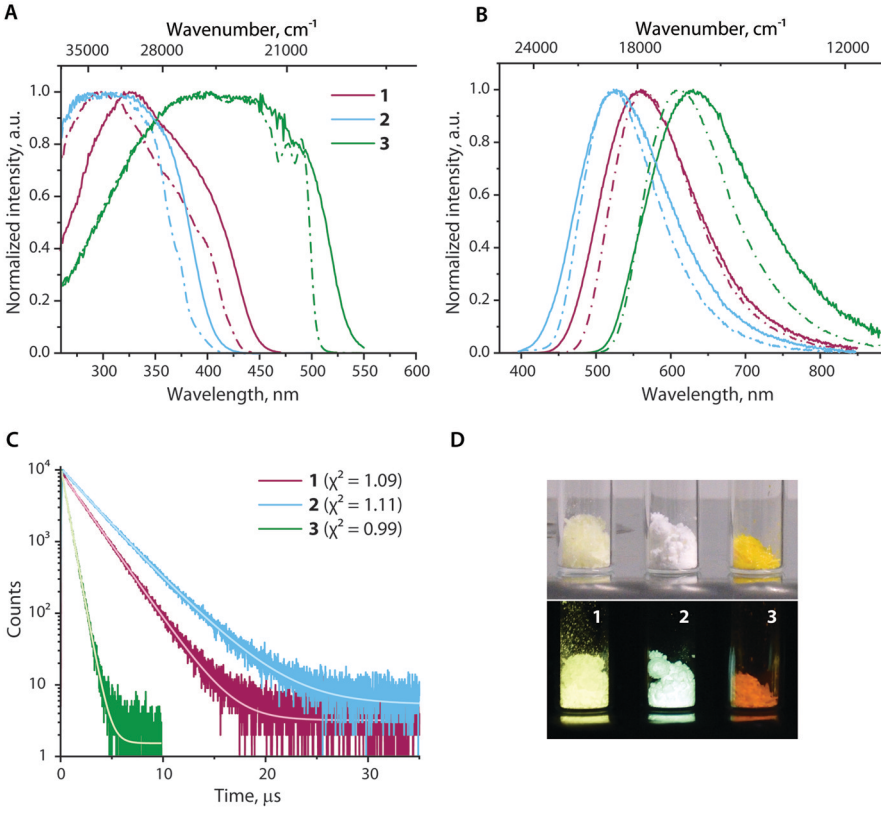

Figure 4. Normalized excitation (A) and emission (B) spectra of compounds **1**–**3** in the solid state at 297 K (solid line) and 77 K (dashed-dotted line); C) time-resolved and fitted decay curves at 297 K; D) images of **1**–**3** under ambient and UV ($\lambda_{exc}=365$ nm) light.

Table 1: Photophysical properties of diphosphonium salts **1–6** in the solid state.

	λ_{exc} [nm]	λ_{em} [nm]	τ_{av} [μs][a]		Φ_{em}		k_r [$\times 10^5$ s^{-1}][b]	
			297 K	77 K	297 K	77 K	297 K	77 K
1	325	560	2.13	3.70	0.54	0.78	2.54	2.11
2	360	520	2.71	5.01	0.75	0.90	2.77	1.84
3	450	645	0.46	2.81	0.07	0.29	1.64	1.04
4	276, 340 sh	515, 555, 600, 650 sh	92.23	745.61	0.13	0.46	0.014	0.006
5	360	460, 490, 525, 565sh	16.60	99.51	0.03	0.17	0.018	0.017
6	467	880	n.d.	n.d.	<0.01	n.d.	n.d.	n.d.

[a] Amplitude-weighted average emission lifetimes for the biexponential decays determined by the equation $\tau_{av}=\Sigma A_i\tau_i$, A_i = weight of the i-th exponent. [b] k_r were estimated by Φ_{em}/τ_{av}.

at 77 K (Figure 5). The peak maxima found at 555 (**4**), 490 (**5**), and 880 (**6**) nm correlated with the variation in the central fragment, the quantum yields in this sequence decreased from 0.13 (**4**) to less than 0.01 (**6**). The lifetimes for **4** and **5** were 92.23 and 16.60 μs at 297 K (we could not determine τ accurately for **6** due to the low emission intensity of NIR emission) resulting in radiative rates of $1.4\times10^3\ s^{-1}$ and $1.8\times10^3\ s^{-1}$. These data are not exceptional for organic phosphors and suggest that $^3\pi$-π^* triplet excited states likely occur for compounds **4–6**. Despite the lack of time-resolved data for **6**, we assume that its

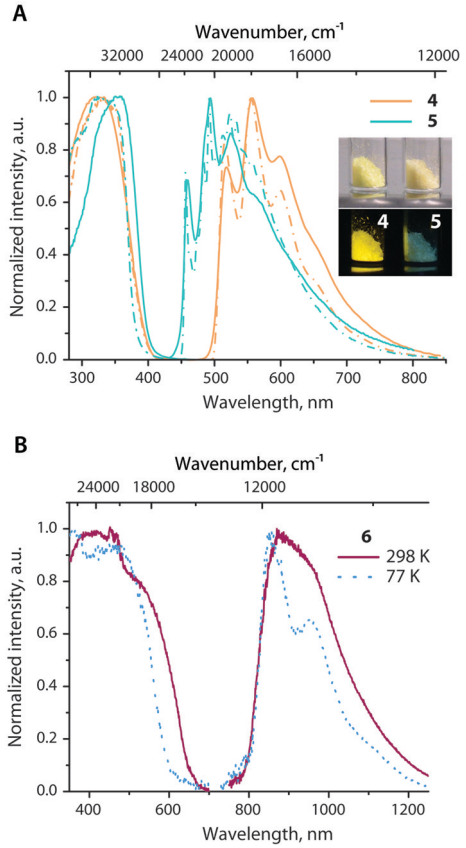

Figure 5. Normalized excitation and emission spectra of compounds **4**, **5** (A) and **6** (B) in the solid state at 297 K (solid line) and 77 K (dashed-dotted line); the photo shows images of **4** and **5** under ambient and UV ($\lambda_{exc}=365$ nm) light.

luminescence is of a triplet nature too because of the significantly lower emission energy compared to those of green-yellow fluorescent anthracene bis(oxo-/thiophosphorane) analogs.[26]

The k_r values for **1–3**, which are two orders of magnitude higher than those for **4** and **5**, are typically expected for late transition metal complexes.[1b,28] Organic luminophores allow harvesting of the triplet excited state and can achieve fast radiative decay via a thermally activated delayed fluorescence mechanism (TADF).[29] Finally, symmetry-forbidden prompt fluorescence can potentially be another alternative for realizing a k_r on the order of 10^6 or less.[30] To decipher the possible scenarios of excited state dynamics for **1–3**, we carried out a systematic variable-temperature study and computational analysis.

Emission mechanism. According to the variable temperature (VT) excitation and emission spectra of **1–3**, the ground states of these species may have different local minima, whereas the excited states of **1** and **2** are virtually unaffected with changes in temperature (Figures 4 and S6). The radiative rates for crystalline **1–3** decreased by 17–37 % upon cooling to 77 K (Table 1, Figure S8). Importantly, the measurements performed for **1** at 5 K did not disclose any additional emission band or a dramatic alteration in the lifetime scale ($\tau_{av}=7.7$ μs at 5 K, Figure S9). These observations, and the structureless emission profiles, indicate that salts **1** and **2** display phosphorescence of charge transfer origin. The absence of prompt fluorescence at 297 K, which is often detected in organic TADF emitters,[29a,31] and no substantial elongation of the lifetime at 77 K, which is expected for transition metal complexes with TADF,[32] allowed to rule out an appreciable contribution of thermally activated delayed fluorescence for **1** and **2**. The luminescence behaviour of **3**, manifested by a blue shift of the emission maximum at 77 K, tentatively arose from the triplet excited state, but was affected by a certain phase transition at low temperature. The pure change in the electronic state (e.g., from S_1 to T_1 that would account for the TADF) cannot explain the detected increase in the emission energy.

The temperature-dependent spectra of **4** exhibited minor variations, whereas **5** demonstrated some growth of a low energy signal near 575 nm in the range of 150–200 K, which could indicate a non-negligible contribution

from CT transitions (Figure S10). The nearly linear growth of the observed lifetimes for **4** and **5** was associated with an increase in the quantum yield and suppression of non-radiative decays at lower temperature, whereas the radiative rates did not fluctuate substantially (Table 1). The long-lived luminescence of crystalline **1–5** under ambient conditions with only microsecond lifetimes suggests efficient ISC, the rate of which is sufficient to overcome the rate of radiative relaxation of the S_1 state.

To support the experiment-based assignment of the origin of the photophysics of **1–6**, we optimized the anion-cation pair models using the QM/MM method, which prevents large scale geometric relaxation and simulates the restrictions imposed by a real solid-state environment. Transition energies and radiative rates were estimated using single-point TD-DFT calculations. These parameters are sensitive to shifts in the energy of the states.[18] For the studied ionic species, the computed rate constants and wavelengths visibly depended on the position of the counterions (relaxed or fixed coordinates, Table S5), and the use of a solvent layer, without which very low transition energies were obtained. Therefore, the calculated data, which were extrapolated from the molecular level to ordered crystal systems, should be treated with caution, and discussed semi-quantitatively.

In line with solid state absorption spectra, the lowest energy excitations for **1–6** mainly involve iodide→π* CT, which correlates with the HOMO and LUMO distributions (Figures 6, S11 and S12). The predicted $T_1 \rightarrow S_0$ radiative transitions are of CT origin for compounds **1–3**, but predominantly have a π-π* character for **4–6**, which is in accordance with the experiment. The orbital configuration of the S_1 and T_1 CT states for **1–3** are not identical and have a hybrid nature with some π-π* contribution that should lead to a non-zero SOC. The non-negligible overlap between S_1 and T_1 accounts for the moderate $\Delta E(S_1\text{-}T_1)$ energy gaps (Table S5). The calculated SOC constants $\xi(S_1,T_1)$ for **1–3** ranged from 156/232 to 413/395 cm^{-1} (frozen/relaxed anions) and were comparable to the corresponding magnitudes reported for some donor-functionalized phosphonium bromides and iodides.[13d,14] The $\xi(S_1,T_1)$ values for **1–3** were probably overestimated considering the similarity of the electronic distribution for the S_1 and T_1 states. Nevertheless, one might expect relatively fast rates of ISC, surpassing those of prompt $S_1 \rightarrow S_0$ fluorescence, due to the appreciable spin-orbit coupling integral $k_{ISC}^{m}(T) \propto \langle \psi_0^{1(0)} | H_{SO} | \psi_m^{3(0)} \rangle^2 \times FCWD$, where *FCWD* denotes the Franck–Condon-weighted density for the $S_1 \rightarrow T_m$ non-radiative transition)[1b] arising from the enhancement of SOC by external HAE of the iodides. No less important factor giving preference to the ISC pathway, are slow rates of fluorescence. These were calculated to be on the order of 10^5–10^6 s^{-1} (Table S5), resulting from the small overlap of the initial and final electronic wavefunctions of the CT transitions $k_f \propto \langle \psi_0^{1(0)} | r | \psi_1^{1(0)} \rangle^2$, where r is the transition dipole length).[1b] In the case of such slow $S_1 \rightarrow S_0$ relaxation even moderate k_{ISC} would be sufficient for the population of the T_1 state. Materials **1–3** thus demonstrate the rare phenomenon of realizing an ^{3}CT(anion-π) state, as exemplified by the earlier pyromellitic diimide iodide.[12e]

The calculated rates of CT phosphorescence (Table S5) for **1–3** were on the order of 10^5 s^{-1} (cf. $k_{r(obs)} = 1.64\text{–}2.77 \times 10^5$ s^{-1}). In **4–6**, the radiative rates were predicted to be 10^2–10^3 times lower (cf. $k_{r(obs)} = 1.4\text{–}1.8 \times 10^3$ s^{-1}), which one might anticipate for the ^{3}π-π* excited state and the external HAE.[1b] Fast radiative relaxation $T_1 \rightarrow S_0$ $\left(k_p \propto \bar{\nu}_0^2 |\overline{\mu_{T_1 \rightarrow S_0}}|^2\right)$ is associated with a large transition dipole moment $\mu_{T1\text{-}S0}$, which is mainly governed by the dipole moment of the fluorescence from an S_m state coupled with the T_1 state ($\overline{\mu_{T_1 \rightarrow S_0}} \propto \mu_{S_m \rightarrow S_0} \langle \psi_1^{3(0)} | H_{SO} | \psi_1^{3(0)} \rangle / (^3E_1 - {}^1E_m)$).[1b] For example, in compound **1**, the strong SOC between T_1 and S_2/S_3 ($\xi(T_1,S_{m=2,3}) > 10^3$ cm^{-1}) was accompanied by fairly high oscillator strengths for $S_m \rightarrow S_0$ ($f = 0.007$ and 0.07 for S_2 and S_3) at a somewhat distorted T_1 geometry. This is expected to facilitate exceptionally high rates of metal-free phosphorescence. Room temperature radiative decays for dicationic species **1** and **2** are very rare among (element)-organic triplet emitters and are close to the fastest organic phosphors with k_r up to 3.33×10^5 s^{-1} reported for hexakis(arylthio)benzenes.[4a]

The importance of iodide anions in attaining phosphorescence was confirmed by the non-emissive character of the triflate salt **1**[OTf]. Although compounds **1–3** and **4–6** with drastically different scales of radiative rates demonstrate distinct structural discrepancies in terms of anion-π contacts, they may not be the only decisive feature of crystal packing responsible for the unusual photophysical behavior of **1–3**. For comparison, we prepared salt [PPh_3Me]I, for which moderately intense phosphorescence at 298 K has been reported ($\lambda_{em} = 487$ nm, $\tau_{obs} = 3.4$ μs, $\Phi_{em} = 0.26$, $k_r = 0.76 \times 10^5$ s^{-1}),[15] although without an exact description of the studied

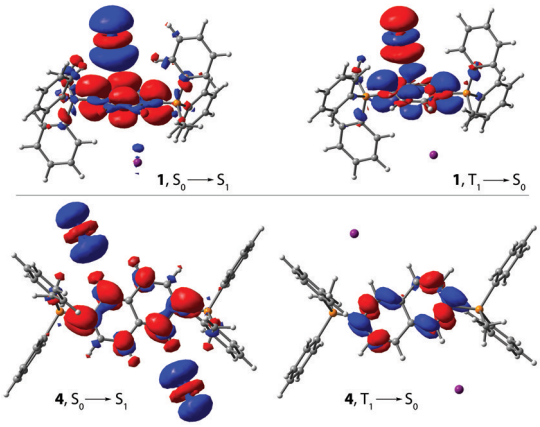

Figure 6. Excitation ($S_0 \rightarrow S_1$) and triplet emission ($T_1 \rightarrow S_0$) electron density difference plots for salts **1** and **4** (isovalue of 0.002 a.u.). During the electronic transition, the electron density decreases in the blue areas and increases in the red areas.

crystalline form. A solvent-free modification (CCDC 1977060)[33] was obtained from a water solution, and its identity was confirmed by XRD analysis. The photoemission data of the ground microcrystalline sample (λ_{em} = 492 nm, τ_{obs} = 2.1 μs, Φ_{em} = 0.17, $k_r = 0.81 \times 10^5\ s^{-1}$, Figure S13) generally match those listed in the earlier publication and indicate a fast radiative rate of emission.[15] The molecular arrangement in the crystal of [PPh_3Me]I shows the shortest anion-π separation of 4.80 Å, which is visibly longer than those observed for **1**–**3**, and at less favorable geometry (the angle between the vertical and iodide-centroid line is 32°) (Figure S13). This is expected to diminish the HAE in [PPh_3Me]I and could be the reason for the 2–3 times lower k_r compared to that of **1**–**3**. However, the efficiency of the anion-π CT and its role in the rates of the ISC and $T_1 \rightarrow S_0$ radiative decay are likely regulated by a more complicated set of structural and electronic factors.

Conclusion

In summary, we report a series of luminescent diphosphonium iodide salts that were readily synthesized from accessible tertiary bisphosphanes, containing an aromatic backbone. The variability of the latter motif (phenylene, naphthalene, biphenyl, and anthracene), which acts as a chromophore center, allows for efficient tuning of the photophysical properties of these species. In polar solutions, the optical behavior of the studied compounds is defined by organic cations showing prompt fluorescence associated with locally excited (π-π*) states. In contrast, the photoluminescence mechanism of crystalline solids strongly depends on anion-π interactions. In the case of iodide-π charge transfer, our theoretical analysis predicted relatively slow rates of prompt fluorescence and fairly strong SOC enhanced by the external heavy atom effect of the anions. This combination favors the population of the triplet excited state, which can undergo radiative relaxation resulting in pure phosphorescence. Remarkably, under the condition of dominating the CT character of the $T_1 \rightarrow S_0$ transition, high quantum yields (Φ_{em} up to 0.75) and fast radiative rate constants (k_r of up to $2.77 \times 10^5\ s^{-1}$) were realized at room temperature for 1,4-phenylene and 1,4-naphthalene substituted compounds. The distortions of the excited state geometry, together with the electrostatically controlled packing effects in these ionic solids, likely play a key role in the enhancement of the transition dipoles, resulting in anomalously fast phosphorescence. Such high rates of radiative processes involving the triplet state can be obtained for organic emitters by means of the TADF mechanism but they remain exceptionally rare for metal-free $T_1 \rightarrow S_0$ relaxation. Thus, the described ionic luminophores can compete with 4d/5d metal complexes. Harnessing CT and external HAE is a new design strategy beyond transition metals and organic delayed fluorophores. Even though the observed phenomenon of fast phosphorescence is found in some crystalline materials and depends on the crystal packing, which is currently of fundamental importance, we believe it can be potentially used in various (mechano)responsive systems where the nature and distance to the anion determine the emission mechanism and the associated optical characteristics. Additional benefits are anticipated from the fabrication of soft and polymeric ionic materials,[34] which can be applied in anticounterfeiting, data encryption, and optoelectronics.

Supporting Information

The authors have cited additional references within the Supporting Information.[35]

Acknowledgements

Financial support from the Academy of Finland (decision 351618, I.O.K.; decision 340584, T.E. and A.J.K.; decision 339544, J.J.S.; Flagship Programme, Photonics Research and Innovation PREIN, decision 320166), Alexander von Humboldt and Otto A. Malm Foundations (A.B.), and the National Science and Technology Council (NSTC), Taiwan, are gratefully acknowledged.

Conflict of Interest

The authors declare no conflict of interest.

Data Availability Statement

The data are available from Cambridge Crystallographic Data Centre (https://www.ccdc.cam.ac.uk/structures/), in the Supporting Information, and from the authors on request.

Keywords: Anion-π Interactions · Charge Transfer · Crystal Engineering · Phosphonium Salt · Phosphorescence

[1] a) S. Mukherjee, P. Thilagar, *Chem. Commun.* **2015**, *51*, 10988–11003; b) S. Hirata, *Adv. Opt. Mater.* **2017**, *5*, 1700116; c) Kenry, C. Chen, B. Liu, *Nat. Commun.* **2019**, *10*, 2111; d) A. D. Nidhankar, Goudappagouda, V. C. Wakchaure, S. S. Babu, *Chem. Sci.* **2021**, *12*, 4216–4236.

[2] a) W. Z. Yuan, X. Y. Shen, H. Zhao, J. W. Y. Lam, L. Tang, P. Lu, C. Wang, Y. Liu, Z. Wang, Q. Zheng, J. Z. Sun, Y. Ma, B. Z. Tang, *J. Phys. Chem. C* **2010**, *114*, 6090–6099; b) W. Zhao, Z. He, J. W. Y. Lam, Q. Peng, H. Ma, Z. Shuai, G. Bai, J. Hao, B. Z. Tang, *Chem* **2016**, *1*, 592–602; c) C. Chen, R. Huang, A. S. Batsanov, P. Pander, Y.-T. Hsu, Z. Chi, F. B. Dias, M. R. Bryce, *Angew. Chem. Int. Ed.* **2018**, *57*, 16407–16411; d) E. Hamzehpoor, D. F. Perepichka, *Angew. Chem. Int. Ed.* **2020**, *59*, 9977–9981; e) Z. Ruan, Q. Liao, Q. Dang, X. Chen, C. Deng, Z. Gao, J. Lin, S. Liu, Y. Chen, Z. Tian, Z. Li, *Adv. Opt. Mater.* **2021**, *9*, 2001549.

[3] a) R. Boonsin, G. Chadeyron, J.-P. Roblin, D. Boyer, R. Mahiou, *J. Mater. Chem. C* **2015**, *3*, 9580–9587; b) L. Yue, Y.

Wang, J. Ma, S. Yuan, S. Xue, Q. Sun, W. Yang, *Mater. Chem. Front.* **2021**, *5*, 5497–5502.
[4] a) A. Fermi, G. Bergamini, R. Peresutti, E. Marchi, M. Roy, P. Ceroni, M. Gingras, *Dyes Pigm.* **2014**, *110*, 113–122; b) B. Xu, H. Wu, J. Chen, Z. Yang, Z. Yang, Y.-C. Wu, Y. Zhang, C. Jin, P.-Y. Lu, Z. Chi, S. Liu, J. Xu, M. Aldred, *Chem. Sci.* **2017**, *8*, 1909–1914; c) M. Shimizu, S. Nagano, T. Kinoshita, *Chem. Eur. J.* **2020**, *26*, 5162–5167.
[5] a) H. Thomas, D. L. Pastoetter, M. Gmelch, T. Achenbach, A. Schlögl, M. Louis, X. Feng, S. Reineke, *Adv. Mater.* **2020**, *32*, 2000880; b) P. She, J. Duan, J. Lu, Y. Qin, F. Li, C. Liu, S. Liu, Y. Ma, Q. Zhao, *Adv. Opt. Mater.* **2022**, *10*, 2102706.
[6] a) R. Pashazadeh, P. Pander, A. Bucinskas, P. J. Skabara, F. B. Dias, J. V. Grazulevicius, *Chem. Commun.* **2018**, *54*, 13857–13860; b) S.-J. Woo, Y.-H. Kim, J.-J. Kim, *Chem. Mater.* **2021**, *33*, 5618–5630; c) B. Sk, S. Sharma, A. James, S. Kundu, A. Patra, *J. Mater. Chem. C* **2020**, *8*, 12943–12950.
[7] a) Z. Yang, C. Xu, W. Li, Z. Mao, X. Ge, Q. Huang, H. Deng, J. Zhao, F. L. Gu, Y. Zhang, Z. Chi, *Angew. Chem. Int. Ed.* **2020**, *59*, 17451–17455; b) X.-K. Ma, W. Zhang, Z. Liu, H. Zhang, B. Zhang, Y. Liu, *Adv. Mater.* **2021**, *33*, 2007476.
[8] a) M. Baroncini, G. Bergamini, P. Ceroni, *Chem. Commun.* **2017**, *53*, 2081–2093; b) A. Forni, E. Lucenti, C. Botta, E. Cariati, *J. Mater. Chem. C* **2018**, *6*, 4603–4626; c) H. Sun, R. Ding, S. Lv, S. Zhou, S. Guo, Z. Qian, H. Feng, *J. Phys. Chem. Lett.* **2020**, *11*, 4962–4969.
[9] a) D. R. Lee, K. H. Lee, W. Shao, C. L. Kim, J. Kim, J. Y. Lee, *Chem. Mater.* **2020**, *32*, 2583–2592; b) W. Shao, H. Jiang, R. Ansari, P. M. Zimmerman, J. Kim, *Chem. Sci.* **2022**, *13*, 789–797.
[10] P. Xue, P. Wang, P. Chen, B. Yao, P. Gong, J. Sun, Z. Zhang, R. Lu, *Chem. Sci.* **2017**, *8*, 6060–6065.
[11] a) O. Bolton, K. Lee, H.-J. Kim, K. Y. Lin, J. Kim, *Nat. Chem.* **2011**, *3*, 205–2010; b) J. Zhou, L. Stojanović, A. A. Berezin, T. Battisti, A. Gill, B. M. Kariuki, D. Bonifazi, R. Crespo-Otero, M. R. Wasielewski, Y.-L. Wu, *Chem. Sci.* **2021**, *12*, 767–773; c) S. Garain, S. Kuila, B. C. Garain, M. Kataria, A. Borah, S. K. Pati, S. J. George, *Angew. Chem. Int. Ed.* **2021**, *60*, 12323–12327; d) W. Dai, X. Niu, X. Wu, Y. Ren, Y. Zhang, G. Li, H. Su, Y. Lei, J. Xiao, J. Shi, B. Tong, Z. Cai, Y. Dong, *Angew. Chem. Int. Ed.* **2022**, *61*, e202200236.
[12] a) J. Wang, X. Gu, H. Ma, Q. Peng, X. Huang, X. Zheng, S. H. P. Sung, G. Shan, J. W. Y. Lam, Z. Shuai, B. Z. Tang, *Nat. Commun.* **2018**, *9*, 2963; b) H. Hu, F. Meier, D. Zhao, Y. Abe, Y. Gao, B. Chen, T. Salim, E. E. M. Chia, X. Qiao, C. Deibel, Y. M. Lam, *Adv. Mater.* **2018**, *30*, 1707621; c) S. Yang, D. Wu, W. Gong, Q. Huang, H. Zhen, Q. Ling, Z. Lin, *Chem. Sci.* **2018**, *9*, 8975–8981; d) Z.-Y. Zhang, Y. Chen, Y. Liu, *Angew. Chem. Int. Ed.* **2019**, *58*, 6028–6032; e) S. Garain, S. M. Wagalgave, A. A. Kongasseri, B. C. Garain, S. N. Ansari, G. Sardar, D. Kabra, S. K. Pati, S. J. George, *J. Am. Chem. Soc.* **2022**, *144*, 10854–10861.
[13] a) G. Chen, S. Guo, H. Feng, Z. Qian, *J. Mater. Chem. C* **2019**, *7*, 14535–14542; b) L.-J. Xu, A. Plaviak, X. Lin, M. Worku, Q. He, M. Chaaban, B. J. Kim, B. Ma, *Angew. Chem. Int. Ed.* **2020**, *59*, 23067–23071; c) P. Alam, N. L. C. Leung, J. Liu, T. S. Cheung, X. Zhang, Z. He, R. T. K. Kwok, J. W. Y. Lam, H. H. Y. Sung, I. D. Williams, C. C. S. Chan, K. S. Wong, Q. Peng, B. Z. Tang, *Adv. Mater.* **2020**, *32*, 2001026; d) P. Alam, T. S. Cheung, N. L. C. Leung, J. Zhang, J. Guo, L. Du, R. T. K. Kwok, J. W. Y. Lam, Z. Zeng, D. L. Phillips, H. H. Y. Sung, I. D. Williams, B. Z. Tang, *J. Am. Chem. Soc.* **2022**, *144*, 3050–3062; e) Y.-S. Wang, T. Zhao, J.-H. Song, X.-D. Tao, D.-H. Zhang, L. Meng, X.-L. Chen, C.-Z. Lu, *Chem. Eng. J.* **2023**, *460*, 141836; f) J. Wei, C. Liu, J. Duan, A. Shao, J. Li, J. Li, W. Gu, Z. Li, S. Liu, Y. Ma, W. Huang, Q. Zhao, *Nat. Commun.* **2023**, *14*, 627.
[14] P. She, Y. Yu, Y. Qin, Y. Zhang, F. Li, Y. Ma, S. Liu, W. Huang, Q. Zhao, *Adv. Opt. Mater.* **2020**, *8*, 1901437.
[15] G. Chen, H. Feng, F. Feng, P. Xu, J. Xu, S. Pan, Z. Qian, *J. Phys. Chem. Lett.* **2018**, *9*, 6305–6311.
[16] G. Bergamini, A. Fermi, C. Botta, U. Giovanella, S. Di Motta, F. Negri, R. Peresutti, M. Gingras, P. Ceroni, *J. Mater. Chem. C* **2013**, *1*, 2717–2724.
[17] a) A. Belyaev, P.-T. Chou, I. O. Koshevoy, *Chem. Eur. J.* **2021**, *27*, 537–552; b) A. Belyaev, Y.-H. Cheng, Z.-Y. Liu, A. J. Karttunen, P.-T. Chou, I. O. Koshevoy, *Angew. Chem. Int. Ed.* **2019**, *58*, 13456–13465.
[18] C. M. Marian, *Annu. Rev. Phys. Chem.* **2021**, *72*, 617–640.
[19] a) R. A. Baldwin, M. T. Cheng, *J. Org. Chem.* **1967**, *32*, 1572–1577; b) D. F. Brayton, D. M. Heinekey, *Organometallics* **2008**, *27*, 3901–3906.
[20] A. Belyaev, I. Kolesnikov, A. S. Melnikov, V. V. Gurzhiy, S. P. Tunik, I. O. Koshevoy, *New J. Chem.* **2019**, *43*, 13741–13750.
[21] J. H. K. Yip, J. Prabhavathy, *Angew. Chem. Int. Ed.* **2001**, *40*, 2159–2162.
[22] Deposition Numbers 2206825 (for $\mathbf{1}^{\mathbf{D}}$), 2206826 (for $\mathbf{1}^{\mathbf{E}}$), 2206827 (for **1**), 2206828 (for **1**[OTf]), 2206829 (for $\mathbf{2}^{\mathbf{W}}$), 2264399 (for **2**), 2206831 (for **3**), 2206830 (for **4**), 2206832 (for **5**), 2206833 (for **6**) contain the supplementary crystallographic data for this paper. These data are provided free of charge by the joint Cambridge Crystallographic Data Centre and Fachinformationszentrum Karlsruhe Access Structures service.
[23] D. L. Herring, *J. Org. Chem.* **1961**, *26*, 3998–3999.
[24] a) H. T. Chifotides, K. R. Dunbar, *Acc. Chem. Res.* **2013**, *46*, 894–906; b) I. A. Rather, S. A. Wagay, R. Ali, *Coord. Chem. Rev.* **2020**, *415*, 213327.
[25] S. Saha, *Acc. Chem. Res.* **2018**, *51*, 2225–2236.
[26] Z. Fei, N. Kocher, C. J. Mohrschladt, H. Ihmels, D. Stalke, *Angew. Chem. Int. Ed.* **2003**, *42*, 783–787.
[27] S. Kepler, M. Zeller, S. V. Rosokha, *J. Am. Chem. Soc.* **2019**, *141*, 9338–9348.
[28] a) H. Yersin, A. F. Rausch, R. Czerwieniec, T. Hofbeck, T. Fischer, *Coord. Chem. Rev.* **2011**, *255*, 2622–2652; b) P.-T. Chou, Y. Chi, M.-W. Chung, C.-C. Lin, *Coord. Chem. Rev.* **2011**, *255*, 2653–2665.
[29] a) Z. Yang, Z. Mao, Z. Xie, Y. Zhang, S. Liu, J. Zhao, J. Xu, Z. Chi, M. P. Aldred, *Chem. Soc. Rev.* **2017**, *46*, 915–1016; b) F.-M. Xie, J.-X. Zhou, Y.-Q. Li, J.-X. Tang, *J. Mater. Chem. C* **2020**, *8*, 9476–9494.
[30] A. G. Crawford, A. D. Dwyer, Z. Liu, A. Steffen, A. Beeby, L.-O. Pålsson, D. J. Tozer, T. B. Marder, *J. Am. Chem. Soc.* **2011**, *133*, 13349–13362.
[31] Y. Liu, C. Li, Z. Ren, S. Yan, M. R. Bryce, *Nat. Rev. Mater.* **2018**, *3*, 18020.
[32] a) R. Czerwieniec, M. J. Leitl, H. H. H. Homeier, H. Yersin, *Coord. Chem. Rev.* **2016**, *325*, 2–28; b) Z. Han, X.-Y. Dong, S.-Q. Zang, *Adv. Opt. Mater.* **2021**, *9*, 2100081.
[33] P. She, Y. Qin, Y. Ma, F. Li, J. Lu, P. Dai, H. Hu, X. Liu, S. Liu, W. Huang, Q. Zhao, *Sci. China Mater.* **2021**, *64*, 1485–1494.
[34] a) Y.-Y. Hu, X.-Y. Dai, X. Dong, M. Huo, Y. Liu, *Angew. Chem. Int. Ed.* **2022**, *61*, e202213097; b) C. Wang, Y. Zhang, Z. Wang, Y. Zheng, X. Zheng, L. Gao, Q. Zhou, J. Hao, B. Pi, Q. Li, C. Yang, Y. Li, K. Wang, Y. Zhao, *Adv. Funct. Mater.* **2022**, *32*, 2111941.
[35] a) *APEX2—Software Suite for Crystallographic Programs*, Bruker AXS, Inc., Madison, WI, USA, **2010**; b) G. M. Sheldrick, *SADABS-2008/1—Bruker AXS Area Detector Scaling and Absorption Correction*, Bruker AXS, Madison, Wisconsin, USA, **2008**; c) G. M. Sheldrick, *Acta Crystallogr. Sect. C* **2015**, *71*, 3–8; d) L. J. Farrugia, *J. Appl. Crystallogr.* **2012**, *45*, 849–854; e) F. Neese, *Wiley Interdiscip. Rev.: Comput. Mol. Sci.* **2022**, *11*, e1606; f) M. A. Rohrdanz, K. M. Martins, J. M.

Herbert, *J. Chem. Phys.* **2009**, *130*, 054112; g) F. Weigend, R. Ahlrichs, *Phys. Chem. Chem. Phys.* **2005**, *7*, 3297–3305; h) F. Neese, *J. Comput. Chem.* **2003**, *24*, 1740–1747; i) F. Neese, F. Wennmohs, A. Hansen, U. Becker, *Chem. Phys.* **2009**, *356*, 98–109; j) V. Barone, M. Cossi, *J. Phys. Chem. A* **1998**, *102*, 1995–2001; k) E. v. Lenthe, E. J. Baerends, J. G. Snijders, *J. Chem. Phys.* **1993**, *99*, 4597–4610; l) C. van Wüllen, *J. Chem. Phys.* **1998**, *109*, 392–399; m) B. de Souza, G. Farias, F. Neese, R. Izsák, *J. Chem. Theory Comput.* **2019**, *15*, 1896–1904; n) J. D. Rolfes, F. Neese, D. A. Pantazis, *J. Comput. Chem.* **2020**, *41*, 1842–1849; o) R. C. Hilborn, *Am. J. Phys.* **1982**, *50*, 982–986; p) R. Dovesi, A. Erba, R. Orlando, C. M. Zicovich-Wilson, B. Civalleri, L. Maschio, M. Rérat, S. Casassa, J. Baima, S. Salustro, B. Kirtman, *Wiley Interdiscip. Rev.: Comput. Mol. Sci.* **2018**, *8*, e1360; q) J. P. Perdew, K. Burke, M. Ernzerhof, *Phys. Rev. Lett.* **1996**, *77*, 3865–3868; r) C. Adamo, V. Barone, *J. Chem. Phys.* **1999**, *110*, 6158–6170; s) D. Vilela Oliveira, J. Laun, M. F. Peintinger, T. Bredow, *J. Comput. Chem.* **2019**, *40*, 2364–2376; t) H. J. Monkhorst, J. D. Pack, *Phys. Rev. B* **1976**, *13*, 5188–5192.

Manuscript received: April 12, 2023
Accepted manuscript online: May 25, 2023
Version of record online: June 16, 2023